Optical temperature sensor with enhanced sensitivity by employing hybrid waveguides in a silicon Mach-Zehnder interferometer

Guan, Xiaowei; Wang, Xiaoyan; Frandsen, Lars Hagedorn

Published in:
Optics Express

Link to article, DOI:
10.1364/OE.24.016349

Publication date:
2016

Document Version
Publisher's PDF, also known as Version of record

Research Article | Vol. 24, No. 15 | 25 Jul 2016 | OPTICS EXPRESS 16349
Optics EXPRESS

Optical temperature sensor with enhanced sensitivity by employing hybrid waveguides in a silicon Mach-Zehnder interferometer

XIAOWEI GUAN,[1*] XIAOYAN WANG,[1,2] AND LARS H. FRANDSEN[1]

[1]*DTU Fotonik, Department of Photonics Engineering, Technical University of Denmark, 2800 Kgs. Lyngby, Denmark*
[2]*Centre for Optical and Electromagnetic Research (COER), Zhejiang University, Zijingang Campus, Hangzhou 310058, China*
[*]*xgua@fotonik.dtu.dk*

Abstract: We report on a novel design of an on-chip optical temperature sensor based on a Mach-Zehnder interferometer configuration where the two arms consist of hybrid waveguides providing opposite temperature-dependent phase changes to enhance the temperature sensitivity of the sensor. The sensitivity of the fabricated sensor with silicon/polymer hybrid waveguides is measured to be 172 pm/°C, which is two times larger than a conventional all-silicon optical temperature sensor (~80 pm/°C). Moreover, a design with silicon/titanium dioxide hybrid waveguides is by calculation expected to have a sensitivity as high as 775 pm/°C. The proposed design is found to be design-flexible and robust to fabrication errors.

OCIS codes: (130.3120) Integrated optics devices; (130.6010) Sensors; (260.3160) Interference.

References and links

1. Z. K. Nagy and R. D. Braatz, "Advances and new directions in crystallization control," Annu. Rev. Chem. Biomol. Eng. **3**(1), 55–75 (2012).
2. M. Phisalaphong, N. Srirattana, and W. Tanthapanichakoon, "Mathematical modeling to investigate temperature effect on kinetic parameters of ethanol fermentation," Biochem. Eng. J. **28**(1), 36–43 (2006).
3. T.-I. Mheen and T.-W. Kwon, "Effect of temperature and salt concentration on *Kimchi* fermentation," Korean J. Food Sci. Technol. **16**(4), 443–450 (1984).
4. K. Furukawa and K. Ohsuye, "Effect of culture temperature on a recombinant CHO cell line producing a C-terminal α-amidating enzyme," Cytotechnology **26**(2), 153–164 (1998).
5. T. Shimizu, M. Yamato, Y. Isoi, T. Akutsu, T. Setomaru, K. Abe, A. Kikuchi, M. Umezu, and T. Okano, "Fabrication of pulsatile cardiac tissue grafts using a novel 3-dimensional cell sheet manipulation technique and temperature-responsive cell culture surfaces," Circ. Res. **90**(3), E40–E48 (2002).
6. Y.-J. Rao, D. J. Webb, L. Zhang, and I. Bennion, "In-fiber Bragg-grating temperature sensor system for medical applications," J. Lightwave Technol. **15**(5), 779–785 (1997).
7. J. Jung, H. Nam, B. Lee, J. O. Byun, and N. S. Kim, "Fiber Bragg grating temperature sensor with controllable sensitivity," Appl. Opt. **38**(13), 2752–2754 (1999).
8. H. Sun, S. Yang, J. Zhang, Q. Rong, L. Liang, Q. Xu, G. Xiang, D. Feng, Y. Du, Z. Feng, X. Qiao, and M. Hu, "Temperature and refractive index sensing characteristics of an MZI-based multimode fiber-dispersion compensation fiber-multimode fiber structure," Opt. Fiber Technol. **18**(6), 425–429 (2012).
9. M. Sun, B. Xu, X. Dong, and Y. Li, "Optical fiber strain and temperature sensor based on an in-line Mach-Zehnder interferometer using thin-core fiber," Opt. Commun. **285**(18), 3721–3725 (2012).
10. Q. Sun, X. Sun, W. Jia, Z. Xu, H. Luo, D. Liu, and L. Zhang, "Graphene-assisted microfiber for optical-power-based temperature sensor," IEEE Photonics Technol. Lett. **28**(4), 383–386 (2016).
11. G.-D. Kim, H.-S. Lee, C.-H. Park, S.-S. Lee, B. T. Lim, H. K. Bae, and W.-G. Lee, "Silicon photonic temperature sensor employing a ring resonator manufactured using a standard CMOS process," Opt. Express **18**(21), 22215–22221 (2010).
12. H.-S. Lee, G.-D. Kim, W.-J. Kim, S.-S. Lee, and W.-G. Lee, "Tunable-resonator based temperature sensor interrogated through optical power detection," Appl. Phys. Express **4**(10), 102201 (2011).
13. H. Xu, M. Hafezi, J. Fan, J. M. Taylor, G. F. Strouse, and Z. Ahmed, "Ultra-sensitive chip-based photonic temperature sensor using ring resonator structures," Opt. Express **22**(3), 3098–3104 (2014).
14. N. Klimov, M. Berger, and Z. Ahmed, "Towards reproducible ring resonator based temperature sensors," Sens. Transducer **191**(8), 63–66 (2015).
15. R. Boeck, M. Caverley, L. Chrostowski, and N. A. F. Jaeger, "Grating-assisted silicon-on-insulator racetrack resonator reflector," Opt. Express **23**(20), 25509–25522 (2015).

#265376 http://dx.doi.org/10.1364/OE.24.016349
Journal © 2016 Received 18 May 2016; revised 19 Jun 2016; accepted 4 Jul 2016; published 11 Jul 2016

16. N. N. Klimov, S. Mittal, M. Berger, and Z. Ahmed, "On-chip silicon waveguide Bragg grating photonic temperature sensor," Opt. Lett. **40**(17), 3934–3936 (2015).
17. C.-M. Chang and O. Solgaard, "Fano resonances in integrated silicon Bragg reflectors for sensing applications," Opt. Express **21**(22), 27209–27218 (2013).
18. N. Klimov, T. Purdy, and Z. Ahmed, "Fabry-Perrot cavity-based silicon photonic thermometers with ultra-small footprint and high sensitivity," in Advanced Photonics 2015, OSA Technical Digest (online) (Optical Society of America, 2015), paper SeT4C.4.
19. A. Irace and G. Breglio, "All-silicon optical temperature sensor based on Multi-Mode Interference," Opt. Express **11**(22), 2807–2812 (2003).
20. Q. Deng, X. Li, R. Chen, and Z. Zhou, "Low-cost silicon photonic temperature sensor using broadband light source," in The 11th International Conference on Group IV Photonics(IEEE Photonics Society, Paris, France, 2014), p. P23.
21. J. F. Tao, H. Cai, Y. D. Gu, J. Wu, and A. Q. Liu, "Demonstration of a photonic-based linear temperature sensor," IEEE Photonics Technol. Lett. **27**(7), 767–769 (2015).
22. R. Dekker, N. Usechak, M. Forst, and A. Driessen, "Ultrafast nonlinear all-optical processes in silicon-on-insulator waveguides," J. Phys. D Appl. Phys. **40**(14), 249–271 (2007).
23. H.-T. Kim and M. Yu, "Cascaded ring resonator-based temperature sensor with simultaneously enhanced sensitivity and range," Opt. Express **24**(9), 9501–9510 (2016).
24. J. Teng, P. Dumon, W. Bogaerts, H. Zhang, X. Jian, X. Han, M. Zhao, G. Morthier, and R. Baets, "Athermal Silicon-on-insulator ring resonators by overlaying a polymer cladding on narrowed waveguides," Opt. Express **17**(17), 14627–14633 (2009).
25. B. Guha, J. Cardenas, and M. Lipson, "Athermal silicon microring resonators with titanium oxide cladding," Opt. Express **21**(22), 26557–26563 (2013).
26. J.-M. Lee, "Ultrahigh temperature-sensitive silicon MZI with titania cladding," Front. Mater. **2**(36), 1–4 (2015).
27. S. Dwivedi, H. D'heer, and W. Bogaerts, "A compact all-silicon temperature insensitive filter for WDM and bio-sensing applications," IEEE Photonics Technol. Lett. **25**(22), 2167–2170 (2013).
28. B. Yang, Y. Zhu, Y. Jiao, L. Yang, Z. Sheng, S. He, and D. Dai, "S. H and D. Dai, "Compact arrayed waveguide grating devices based on small SU-8 stripe waveguides," J. Lightwave Technol. **29**(13), 2009–2014 (2011).
29. G. Voskerician, M. S. Shive, R. S. Shawgo, H. von Recum, J. M. Anderson, M. J. Cima, and R. Langer, "Biocompatibility and biofouling of MEMS drug delivery devices," Biomaterials **24**(11), 1959–1967 (2003).
30. M. Pu, L. H. Frandsen, H. Ou, K. Yvind, and J. M. Hvam, "Low insertion loss SOI microring resonator integrated with nano-taper couplers," the Conference on Frontiers in Optics (FiO) 2009, FThE1 (2009).
31. J.-M. Lee, "Influence of titania cladding on SOI grating coupler and 5 μm-radius ring resonator," Opt. Commun. **338**, 101–105 (2015).
32. M. Furuhashi, M. Fujiwara, T. Ohshiro, M. Tsutsui, K. Matsubara, M. Taniguchi, S. Takeuchi, and T. Kawai, "Development of microfabricated TiO2 channel waveguides," AIP Adv. **1**(3), 032102 (2011).

1. Introduction

Temperature is a fundamental parameter in many processes ranging from industrial manufacturing to life sciences, e.g., crystallization [1], fermentation for fuel [2] and food [3], and cell culture to produce enzymes [4] and cardiac tissue grafts [5]. So far, the most accessible method for measuring the temperature is still resistance thermometry, in which a metal's resistance varies with the temperature. However, given its problem of being sensitive to electromagnetic interference (EMI), humidity, and mechanical shocks, resistance thermometers' territory is being seized by sensors utilizing other methods, among which optical temperature sensors are attracting substantial interests [6–21]. Optical temperature sensors have been demonstrated in fibers inscribed with Bragg gratings [6, 7] and in configurations of Mach–Zehnder Interferometers (MZIs) [8, 9], or e.g. utilizing graphene [10]. Integrated optical sensors on silicon [11–21] have also been demonstrated and are foreseen to be promising candidates for integration with electronic circuits for on-chip signal processing and calibration compared with their fiber-optic counterparts. Furthermore, the large thermo-optic coefficient (TOC) of silicon (~1.86×10^{-4}/°C [22]) suggests a large temperature sensitivity of the temperature sensor, which is usually preferred in a temperature sensor employed in many chemical or biological processes that may behave distinctively different at small temperature variations [4].

Diverse silicon photonic structures have been utilized to achieve temperature sensors, including ring resonators [11–15], Bragg reflectors [16, 17], Fabry-Perrot (FP) cavities [18], and interferometers [19–21]. However, the temperature sensitivity of above demonstrated sensors are typically limited to ~80 pm/°C. Recently, a silicon optical temperature sensor leveraging the Vernier effect of two cascaded ring resonators was demonstrated [23]. While it achieved an enhanced temperature sensitivity of 293.9 pm/°C, the performances inherently

Optics EXPRESS

depend on the fine tailoring of the free spectral regions (FSRs) of the two rings and, therefore, introduces restrictions to the fabrication tolerance.

In this paper, we propose and experimentally demonstrate a temperature sensor on silicon with an enhanced temperature sensitivity by employing an unbalanced MZI configuration with hybrid waveguides. The two arms of the MZI consist of non-identical optical waveguides providing opposite phase changes of the transmitted modes with respect to the temperature variation. While a silicon nanowire itself having silica or air cladding transmits a mode with a positive temperature-dependent phase change, a negative temperature-dependent phase change can be realized in a waveguide with negative-TOC material as the core. Materials with a negative TOC like polymers [24] and titanium dioxide (TiO_2) [25] have already been utilized as the cladding for a narrowed silicon waveguide to reduce the temperature dependence of the silicon photonic devices, but few reports have been published on utilizing these materials in temperature sensors. Recently, an MZI-based silicon temperature sensor with TiO_2 overlaying both arms have achieved a large temperature sensitivity of −340 pm/°C, since the TiO_2 used in the work has an unexplainably ultrahigh TOC of −5 to -7×10^{-4}/°C [26]. In our work, the negative-TOC material is used as the waveguide core in one arm of the proposed unbalanced MZI-based temperature sensor and, therefore, the temperature-dependent phase differential of the two arms is further intensified. The temperature sensitivity of the proposed device is measured to be 172 pm/°C utilizing silicon (Si) / polymer (SU-8) hybrid waveguides, and is calculated to be as high as 775 pm/°C if we employ Si/TiO_2 hybrid waveguides with the same large TOC of TiO_2 as in [26]. The present design can be much more compact (arm lengths 30 μm) compared with the one proposed in [26], which is longer than 360 μm. Furthermore, our design is found to be quite design-flexible and fabrication-tolerant.

2. Principle and design

In a temperature sensor based on an unbalanced MZI with the two arms denoted as arm 1 and arm 2, the temperature sensitivity S, i.e., the interference wavelength shift with respect to the temperature T, is given by [27]

$$S = \frac{\Delta\lambda}{\Delta T} = \lambda \frac{(\mathrm{d}n_{\mathrm{eff1}} / \mathrm{d}T) \cdot L_1 - (\mathrm{d}n_{\mathrm{eff2}} / \mathrm{d}T) \cdot L_2}{n_{g1} \cdot L_1 - n_{g2} \cdot L_2} \tag{1}$$

where λ is the interference wavelength, L_1 (L_2) is the length of arm 1 (arm 2), n_{g1} (n_{g2}) and n_{eff1} (n_{eff2}) correspond to the group index and the effective index of the mode propagating in arm 1 (arm 2), respectively. To simplify the design, we consider the situation where the two arms are of equal lengths, i.e., $L = L_1 = L_2$. In this way, expression (1) can be written as $S = \lambda \frac{\mathrm{d}n_{\mathrm{eff1}} / \mathrm{d}T - \mathrm{d}n_{\mathrm{eff2}} / \mathrm{d}T}{n_{g1} - n_{g2}}$, and, therefore, is independent on the arm lengths. In order to increase S, one way is to increase the differential of the phase change of the two arms with respect to the temperature, i.e., maximize $\mathrm{d}n_{\mathrm{eff1}}/\mathrm{d}T$- $\mathrm{d}n_{\mathrm{eff2}}/\mathrm{d}T$. This can be done more easily by employing materials with positive and negative TOCs in the waveguide cores in arm 1 and arm 2, respectively.

Following the principle above, we schematically present our design of the MZI-based temperature sensor on silicon in Fig. 1. Light is split into two parts by a power splitter based on a directional coupler and the two parts recombine in a second directional coupler after having propagated along arm 1 and arm 2. For arm 1, the waveguide is a conventional single-mode silicon waveguide with the same width (w_1) as the directional couplers. In arm 2, there is a narrow (w_2<200nm) silicon nanowire in the center with two tapers connecting to the single-mode silicon waveguides with widths w_1. An SU-8 polymer waveguide is covering the narrow nanowire part and the tapers. Here, SU-8 is used because it has a negative TOC (-1.21×10^{-4}/°C) [28], and is easily fabricated and biocompatible [29], which suggests a potential for the proposed temperature sensor to be applied in biosensing applications. The

Optics EXPRESS

lengths of the narrow nanowire and the tapers are denoted as L and L_t, respectively. Inset (a) in Fig. 1 shows the cross-section of arm 1 and the power distribution of the transverse-magnetic (TM) mode. The height of the silicon waveguide is fixed at 250 nm and the upper cladding is air. From the power distribution, one can see that the mode is tightly confined in the silicon and, therefore, has a positive temperature-dependent phase change. Inset (b) in Fig. 1 shows the cross section of the waveguide in the narrow nanowire part of arm 2 and the power distribution of the TM mode is also given for a nanowire width of 40 nm. We use the configuration of having a narrow silicon nanowire overlaid with a SU-8 waveguide cladding rather than having a pure SU-8 waveguide to avoid the losses generated from the abrupt terminals of the tapers. From the power distribution in inset (b), one can see that almost all the light of the mode is leaked to the SU-8 and, hence, will have a negative temperature-dependent phase change.

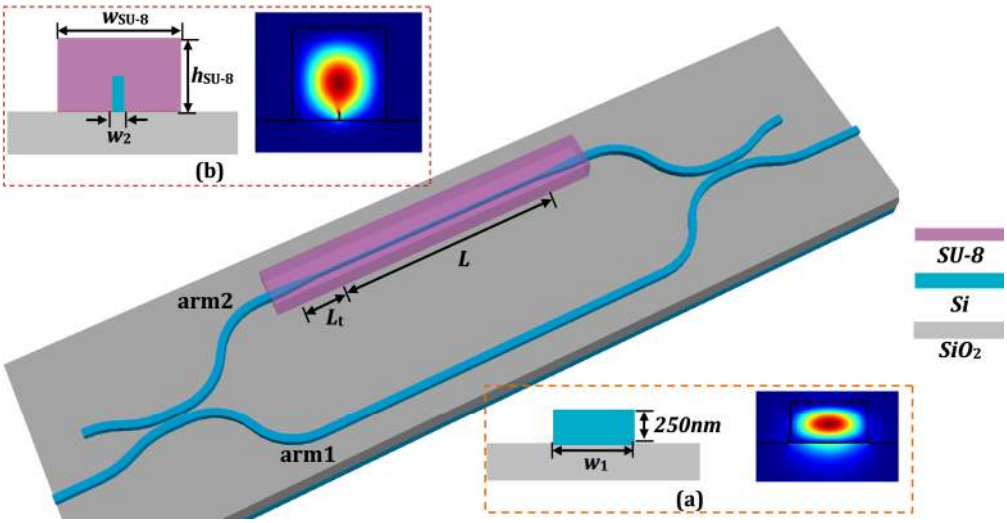

Fig. 1. Schematic of the proposed MZI-based temperature sensor with Si/SU-8 hybrid waveguides. Insets (a) and (b) show the cross section and the mode (power) distribution of the waveguides in arm 1 and in the narrow nanowire part of arm 2, respectively.

Figures 2(a) and 2(b) show the calculated group index (n_g) and the effective index variation with the temperature (dn_{eff}/dT) of the waveguides in arm 1 and arm 2 when the width of the silicon part changes. Here, the wavelength is 1550 nm and the silicon height, the SU-8 height (h_{SU-8}) and the SU-8 width (w_{SU-8}) are fixed at 250 nm, 2930 nm and 3850 nm, respectively. For SU-8, the refractive index and the TOC are 1.574 and -1.21×10^{-4}/°C, respectively [28]. It is reasonable that both the group index and the variation of the effective index with the changing temperature decrease for a smaller silicon width for both arms, since there will be less light confined in the silicon. Particularly, the effective index variation with changing temperature starts to be more and more negative as the silicon width decreases below ~230 nm and reaches the minimum (-1.2×10^{-4}/°C), close to the TOC of SU-8 material. Figures 2(c) and 2(d) show the calculated FSR and the temperature sensitivity S, respectively, of the proposed temperature sensor as a function of the width of the silicon nanowire in arm 2, when the width of arm 1 is fixed at different widths. Here, the FSR is calculated by $FSR = \frac{\lambda^2}{(n_{g1} - n_{g2})L}$ and L is fixed to 190 μm neglecting the length of the tapers. From Fig. 2(d), one can find that the temperature sensitivity generally increases when w_2 increases from ~120 nm and w_1 decreases. Although a larger w_2 and a smaller w_1 will give a higher temperature sensitivity, it will also give a larger FSR as shown by Fig. 2(c), since the differential between n_{g1} and n_{g2} is smaller. Knowing that the spectral output of an MZI has a

Optics EXPRESS

trigonometric shape, a large FSR indicates a tiny power change per unit wavelength change and will impose difficulties on the optical spectral analyzer (OSA) to determine the interference wavelength center during the spectral interrogation. When w_2<120 nm, the temperature sensitivity more or less keeps constant, since almost all the light is localized in the SU-8. In our design, we choose w_1 = 460 nm and w_2 = 40 nm, which gives an FSR of 4.2 nm and a temperature sensitivity S of 158 nm/°C. For the proposed MZI structure, we also tune the coupling length of the input directional coupler in order to achieve a 30% / 70% splitting of power to arm 1 and arm 2, respectively, to account for the 2.6 dB excess loss in the two tapers of arm 2 [30].

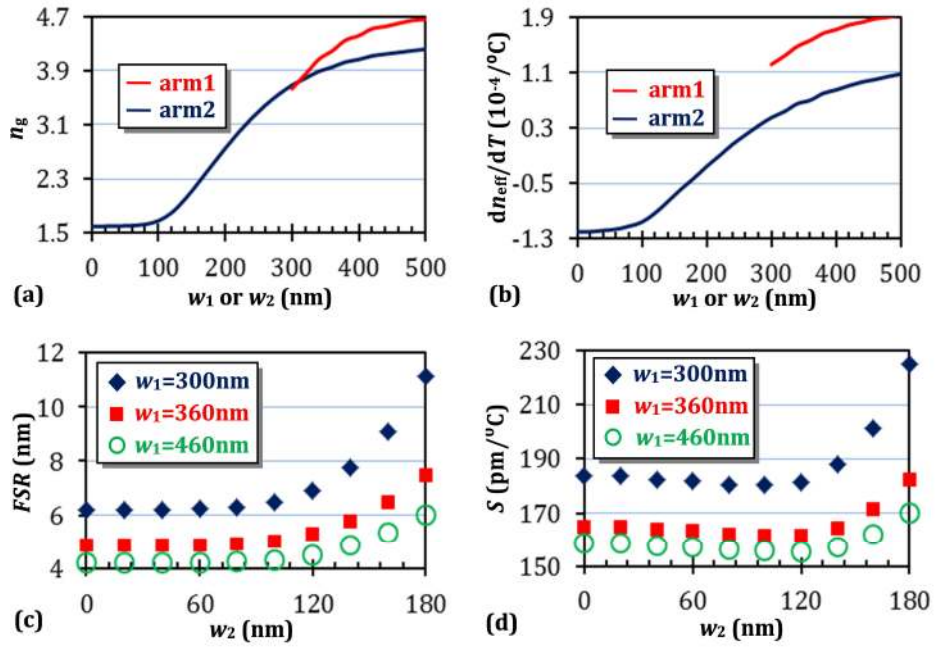

Fig. 2. The group index (a) and the effective index variation with the temperature changes (b) as a function of the waveguide width in arm 1 or arm 2. The FSR (c) and the temperature sensitivity (d) of the proposed temperature sensor as a function of the width of the silicon nanowire in arm 2, when the width of arm 1 is 300 nm (blue diamond), 360nm (red square) and 460 nm (green circle). Here, the wavelength is 1550 nm.

3. Fabrication and measurement

The designed temperature sensor was fabricated in a silicon-on-insulator material having 250 nm of silicon on top of a 3 μm buried-oxide (BOX) layer. Inverse tapers with SU-8 waveguide cladding [30] were used to couple light between tapered and lensed fibers and the silicon waveguides. First-step electron-beam lithography followed by an inductive plasma etching was utilized to pattern the silicon including the MZI and the inverse taper couplers. A 2930-nm thick SU-8 (SU-8 2005, MicroChem) was spin-coated on the chip and the SU-8 structures were selectively defined on the silicon by another electron-beam lithography step. Fig. 3(a) shows a scanning electron microscopy (SEM) image of the fabricated temperature sensor with Si/SU-8 hybrid waveguides. The inset in the green frame in Fig. 3(a) shows the close-up view of the interface part of the Si waveguide and the SU-8 waveguide and one can find that the two waveguides are well-aligned. Since the SU-8 waveguide is quite wider (3850 nm) than the silicon waveguide (460 nm), ultra-precise alignment is not necessary and, therefore, the present design is relatively fabrication tolerant. As a reference for the performances of the proposed temperature sensor with hybrid waveguides, an all-silicon MZI-

Optics EXPRESS

based temperature sensor with an arm length difference of 50 μm was fabricated and is also shown on the SEM image in Fig. 3(b).

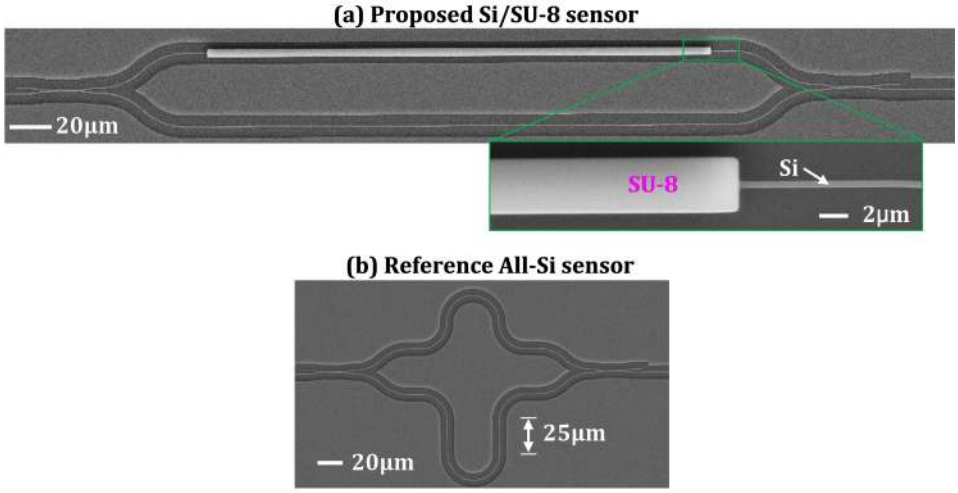

Fig. 3. SEM image of the proposed temperature sensor with (a) Si/SU-8 hybrid waveguides and (b) the all-Si temperature sensor for reference. The inserted SEM image in the green frame in (a) shows the close-up view of the interface part of the Si waveguide and the Si/SU-8 waveguide.

The fabricated sensors were characterized using a tunable laser (AQ4321D, Ando) and an OSA (AQ6317B, Ando) to record the transmission spectra for the sensors. A polarization controller (PC) was used before the sample to select the TM mode. The temperature of the chip was controlled by a temperature feedback system consisting of a semiconductor cooler beneath the sample holder, an integrated precision temperature sensor (LM335) inside the sample holder and a temperature controller (LDC 502, SRS). Figures 4(a) and 4(b) show the measured and normalized spectra of the temperature sensor with Si/SU-8 hybrid waveguides and the all-Si reference temperature sensor at different temperatures, respectively. Here, a silicon straight waveguide with the same fiber-waveguide couplers is utilized for the normalization. As expected, one can see that both the spectra of the proposed and the reference temperature sensors have a red shift with increasing temperature. From Fig. 4(a), one can find the FSR of the proposed temperature sensor to be 4.22 nm, which agrees well with the calculations in Fig. 2(c). The insertion loss for the sensor can also be extracted to be ~1.6 dB. From Fig. 4(b), the FSR of the reference all-Si temperature sensor is found to be ~11 nm, which agrees nicely with a MZI with an arm length difference of 50 μm.

Figure 4(c) gives the interference wavelength shift with respect to the temperature for the proposed (red circle) and the reference (blue square) temperature sensors. Here, the reference wavelengths for the proposed and the reference sensors are 1543.7 nm and 1544.6 at room temperature (24.1 °C), respectively. Linear fittings are also shown to obtain the temperature sensitivities, which are extracted to be 172 pm/°C and 70 pm/°C for the proposed and the reference temperature sensors, respectively. The measured sensitivity of the all-silicon reference temperature sensor agrees well with previous reports [16–18]. Considering the effect of the two tapers with L_t = 20 μm, the calculated temperature sensitivity is 163 pm/°C, which agrees well with the measured sensitivity. For such a measured temperature sensitivity, the proposed sensor has a potential to measure temperature changes as small as 0.006 °C considering that the current setup has a wavelength resolution of 1 pm. The sensing range defined as *FSR*/*S* can be extracted as ~25 °C.

Optics EXPRESS

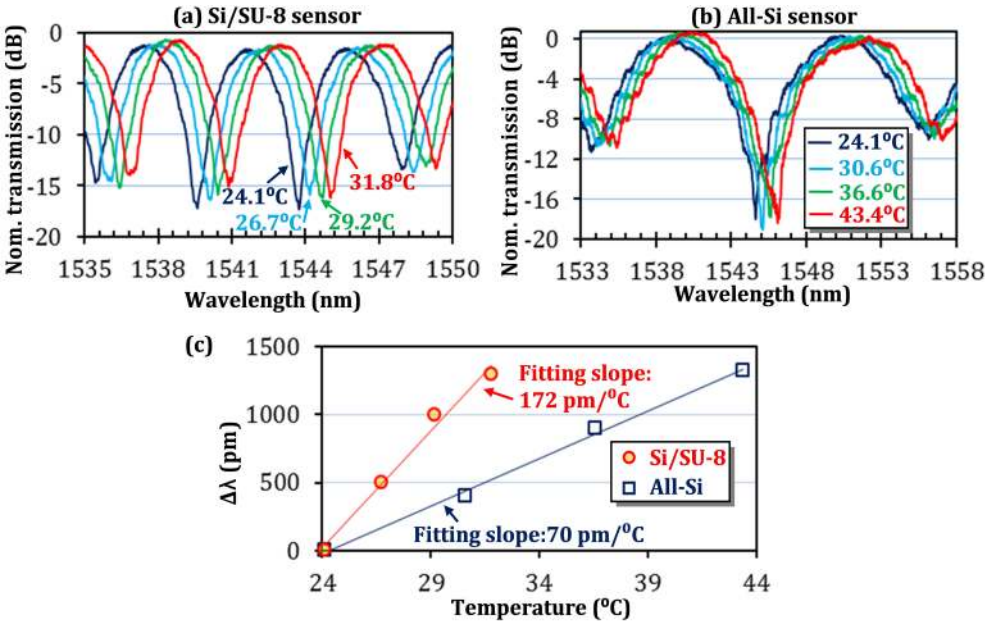

Fig. 4. Measured and normalized spectra of the proposed temperature sensor with (a) Si/SU-8 hybrid waveguides and (b) the reference all-Si temperature sensors recorded at different temperatures. (c) The shift of the interference wavelength as a function of the temperature for the proposed (red circle) and the reference (blue square) sensors. Here, the wavelengths for the proposed and the reference sensors are 1543.7 nm and 1544.6 at 24.1 °C, respectively.

Figure 5 show the measured and normalized spectra of the proposed temperature sensor with Si/SU-8 hybrid waveguides at different temperatures when the silicon narrow nanowire in arm 2 is (a) 40 nm and (b) 90 nm. Here, the length L is increased to 290 μm. From Fig. 5(a), one can find that the temperature sensor has an extinction ratio, an insertion loss, and a temperature sensitivity (171 pm/°C) comparable to the temperature sensor having L = 190 μm in Fig. 4(a). Only the FSR is changed to 2.9 nm due to a different arm length. Therefore, for the present design, it is easy to obtain different sensing ranges, set by the FSR, without degrading the performance by simply tuning the length L. For example, one is expected to obtain a sensing range of ~100 °C by shortening L to 20 μm. Moreover, the undegraded performances shown in Fig. 5(b) for the sensor with w_2 = 90 nm also demonstrates a good fabrication tolerance of the proposed temperature sensor.

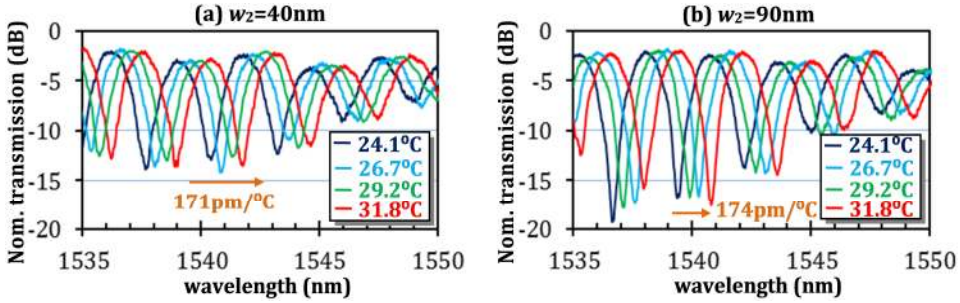

Fig. 5. Measured and normalized spectra of the proposed temperature sensor with Si/SU-8 hybrid waveguides at different temperatures for the width of the narrow nanowire of arm 2 is 40 nm (a) and 90 nm (b), respectively. Here, the length of the narrow nanowire L is 290 μm.

Full CMOS-compatibility is usually desired for mass-productive and low-cost integrated sensors. It is well known that TiO_2 is CMOS-compatible. Moreover, TiO_2 has a negative TOC and, therefore, can be exploited to further increase the sensitivity of our hybrid temperature

Optics EXPRESS

sensor. TiO_2 deposited by different methods and at different temperatures can provide different refractive indices and TOCs as summarized by Lee in [31]. In the following calculations, we use the same refractive index (2.13) and TOC (-7×10^{-4}/°C) of the TiO_2 as in [26]. Replacing the SU-8 in Fig. 1 with TiO_2, we can obtain a full CMOS compatible temperature sensor with Si/TiO_2 hybrid waveguides. Figure 6 presents the calculated FSR and the temperature sensitivity S at the wavelength 1550 nm of the proposed sensor for different TiO_2 waveguide widths (w_{TiO2}) and different TiO_2 waveguide heights (h_{TiO2}). Here, w_2 = 40 nm and in order to get a large FSR (sensing range), we choose a short arm length of 30 μm. It is noteworthy that a longer arm length will not degrade the temperature sensitivity. Also noteworthy, here we use the transverse-electric (TE) mode since for this polarization the TiO_2 does not need to be very thick to confine light in the TiO_2 and, hence, will make the fabrication easier. From Fig. 6, one can find that the temperature sensitivity can be as high as 775 pm/°C when w_{TiO2} = 700 nm and h_{TiO2} = 600 nm. Meanwhile, the corresponding FSR is 43.5 nm and the sensing range is ~56 °C. For the fabrication of the TiO_2 waveguides, one can use dry etching employing a chromium mask as demonstrated in [32].

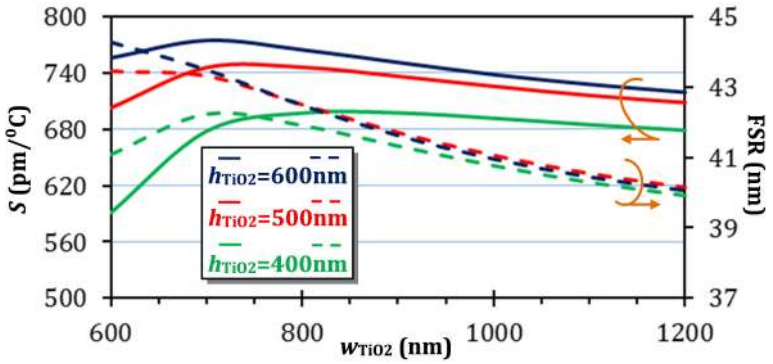

Fig. 6. Calculated FSR and temperature sensitivity of the proposed temperature sensor with Si/TiO_2 hybrid waveguides as a function of the TiO_2 waveguide width at different TiO_2 waveguide heights. Here, the arm lengths are 30 μm and w_2 = 40 nm.

4. Conclusion

In conclusion, we have proposed and experimentally demonstrated a Mach-Zehnder interferometer-based temperature sensor with hybrid waveguides on silicon. In the present design, one arm is silicon waveguide and the other is a hybrid waveguide with a negative thermo-optic coefficient enhancing the temperature sensitivity. A hybrid silicon/SU-8 waveguide is employed to experimentally verify the principle and a temperature sensitivity is measured to be 172 pm/°C, which is two times larger than the reference all-silicon Mach-Zehnder interferometer temperature sensor (70 pm/°C) and the conventional all-silicon temperature sensors with other configurations (~80 pm/°C). Our hybrid design has a good flexibility where one can simply change the arm lengths to obtain different sensing ranges while simultaneously keeping the performances. Temperature sensors with different arm lengths and widths have been fabricated and reveals no obvious performance degradation, which suggests a good fabrication tolerance. Furthermore, the proposed design is calculated to give a temperature sensitivity as high as 775 pm/°C by employing a hybrid silicon/TiO_2 waveguide. This paves the way for full CMOS compatible optical temperature sensors with high sensitivities for use in e.g. bio sensing or chemical analysis.

Acknowledgments

This work was supported by the VILLUM foundation via the project 'Optical Nano-engineered Components for High-capacity Integrated silicon Photonics' (ONCHIP). Xiaoyan Wang acknowledges China Scholarship Council (CSC) for the financial support.